Theor Chem Acc (2010) 126:197–211
DOI 10.1007/s00214-009-0644-7

REGULAR ARTICLE

A theoretical study of the hydration of Rb^+ by Monte Carlo simulations with refined ab initio-based model potentials

María Luisa San-Román · Jorge Hernández-Cobos · Humberto Saint-Martin · Iván Ortega-Blake

Received: 24 June 2009 / Accepted: 14 September 2009 / Published online: 4 October 2009

Abstract An infinitely diluted aqueous solution of Rb^+ was studied using ab initio-based model potentials in classical Monte Carlo simulations to describe its structural and thermodynamic features. An existing flexible and polarizable model [Saint-Martin et al. in J Chem Phys 113(24) 10899, 2000] was used for water–water interactions, and the parameters of the Rb^+–water potential were fitted to reproduce the polarizability of the cation and a sample of ab initio pair interaction energies. It was necessary to calibrate the basis set to be employed as a reference, which resulted in a new determination of the complete basis set (CBS) limit energy of the optimal Rb^+–OH_2 configuration. Good agreement was found for the values produced by the model with ab initio calculations of three- and four-body nonadditive contributions to the energy, as well as with ab initio and experimental data for the energies, the enthalpies and the geometric parameters of $Rb^+(H_2O)_n$ clusters, with $n = 1, 2,\ldots, 8$. Thus validated, the potential was used for simulations of the aqueous solution with three versions of the MCDHO water model; this allowed to assess the relative importance of including flexibility and polarizability in the molecular model. In agreement with experimental data, the Rb^+–O radial distribution function (RDF) showed three maxima, and hence three hydration shells. The average coordination number was found to be 6.9, with a broad distribution from 4 to 12. The dipole moment of the water molecules in the first hydration shell was tilted to 55° with respect to the ion's electric field and had a lower value than the average in bulk water; this latter value was recovered at the second shell. The use of the nonpolarizable version of the MCDHO water model resulted in an enhanced alignment to the ion's electric field, not only in the first, but also in the second hydration shell. The hydration enthalpy was determined from the numerical simulation, taking into account corrections to the interfacial potential and to the spurious effects due to the periodicity imposed by the Ewald sums; the resulting value lied within the range of the various different experimental data. An analysis of the interaction energies between the ion and the water molecules in the different hydration shells and the bulk showed the same partition of the hydration enthalpy as for K^+. The reason for this similarity is that at distances longer than 3 Å, the ion–water interaction is dominated by the charge-(enhanced) dipole term. Thus, it was concluded that starting at K^+, the hydration properties of the heavier alkali metal cations should be very similar.

Keywords Rubidium ion hydration · Polarizable force fields · Monte Carlo simulation

Dedicated to the memory of Professor Jean-Pierre Daudey and published as part of the Daudey Memorial Issue.

M. L. San-Román
Centro de Investigaciones Químicas,
Universidad Autónoma del Estado de Morelos,
Av. Universidad 1001, Col. Chamilpa,
62210 Cuernavaca, Morelos, Mexico

J. Hernández-Cobos · H. Saint-Martin
Instituto de Ciencias Físicas,
Universidad Nacional Autónoma de México,
Apartado Postal 48-3, 62251 Cuernavaca,
Morelos, Mexico

I. Ortega-Blake (✉)
Departamento de Física Aplicada,
Centro de Investigación y Estudios Avanzados,
Unidad Mérida, Cordemex, 97310 Mérida,
Yucatán, Mexico
e-mail: ivan@fis.unam.mx

1 Introduction

Although most of rubidium's chemistry is the same as that of the lighter alkali metals [1], its behavior in solution shows some peculiarities [2–11] that are ascribed to its low charge-to-radius ratio, with consequent more important water–water versus ion–water interactions [12], leading to favorable ion pairing [13–15]. As the hydration of Rb^+ involves both hydrophilic and hydrophobic effects [16], it is intrinsically interesting to attain a reliable molecular image of hydrated Rb^+. Because the experimental determination of single ion hydration properties implies the extrapolation to a hypothetical standard state of infinite dilution of data obtained from solutions of various different concentrations of salts [17], a complementary self-consistent theoretical approach is required to discriminate one type of effect from the other. In the case of Rb^+, the previously mentioned ion pairing hinders the experimental resolution of the hydration properties of individual atoms by ^{87}Rb-NMR [14, 18]. Even the neutron diffraction and X-ray techniques that have been used to study the hydration of Rb^+ [19–34] are limited because it reacts by strong fluorescence to irradiation by beams of the most frequently used wavelengths [35].

No major biological role is known for Rb^+, but the selectivity of some ion channels to Rb^+ is similar to K^+ [36–38]. Selectivity for larger alkali cations is also found in compact smectite clays [39, 40]. Of course, one of the major interests in ion selectivity is to understand the molecular basis of the exquisite selectivity that biological channels present. Several models have been advanced: the snug-fit mechanism [41, 42], the action of the carbonyl's field [43], and particular thermodynamics arising from the coordination properties of the ions [44–49]. These models have been recently tested by comparison to experiment and molecular dynamics calculation of channels in membranes [50, 51] and found that those related to singular behavior due to the coordination properties of the ions are the more viable. Furthermore, selectivity is a result of a fine balance, and therefore accurate description of the coordination properties, including effects such as polarization, is required. As a matter of fact, a comparison of the different descriptions obtained for ion channel simulations with two common force fields, CHARMM [52] and GROMOS96 [53], shows that their differences, E(CHARMM)–E(GROMOS96), are of the same size as the difference in energy that accounts for selectivity [51]. It is therefore necessary to develop potentials that yield an accurate description of the ion's hydration.

The theoretical approach by means of classical numerical simulations with empirical models strongly depends on the available experimental data [54–63]. These problems may be overcome by the alternative of using an approximate method to compute the quantum potential "on-the-fly" during the simulation. In this approach, a fictitious mass is assigned to the electronic wave function, which is described with a density functional and expanded in plane waves [64]. Because the electrons of all the molecules in the system are included in the quantum calculation, the computational cost limits its size to less than 100 water molecules, and the length of the simulation to less than 60 ps. This strategy has been used in simulations of aqueous solutions of the lighter alkali metals [65–68] (see Ref. [69] for a recent review), but not yet for Rb^+. Besides the limitations in system size and simulation length, this approach has been criticized [70] for the dependency of the results on the choice of density functional for the approximate quantum calculations, which may lead to significant disagreement with experimental results [67, 71].

A different strategy is to treat only a region of the system quantum mechanically and the rest classically [72]. The hybrid quantum mechanical/molecular mechanical (QM/MM) method allows for the inclusion of much more water molecules and for the use of more refined ab initio methods than density functional theory (DFT) [70]. The length of the simulation is still limited to less than 60 ps, and the crucial choices include the size of the region to be treated quantum-mechanically, the classical force field to treat the rest of the system, and the coupling between the two descriptions. This strategy has been used in simulations of aqueous solutions of Na^+ and K^+ [73], Cs^+ [71] and of Rb^+ [74], where the ab initio calculations of the ion–water interactions were performed at the double-zeta Hartree-Fock (HF) level, with effective-core potentials (ECP) for the ions. A more refined description of the quantum–classical coupling has been recently reported and christened as *quantum mechanical charge field (QMCF) molecular dynamics* [75]. It was employed in further simulations of Na^+ and K^+ in aqueous solution [76], resulting in small differences with regard to the previous QM/MM simulations [73], and in disagreement with DFT-based molecular dynamics [66, 69]. This discrepancy has been ascribed [69] to the lack of correlation energy in the ab initio calculations of Ref. [73].

A substantial increase in the length of the simulation can be obtained if the quantum treatment is reduced to include only the ion and its first hydration shell, thus defining a hydrated ion complex [77–79], and the coupling to the classical simulation is done through an analytical potential of the hydrated ion with the water molecules [80]. This strategy allows an even higher level of ab initio calculations for the region of interest, but does not permit the exchange of water molecules from the first hydration shell. Therefore, it can only be applied when the residence time of a water molecule in the first hydration shell is substantially long, as is the case for some highly charged cations.

Yet another strategy to include the "correct" quantum interactions in the classical simulation is the design of

ab initio-based analytical model potentials, whose parameters are fitted to reproduce high quality ab initio calculations. The early attempts [81, 82] accounted only for pair interactions, but the more modern potentials include many-body nonadditive contributions [83–85]. The main shortcomings in this case include the accuracy with which the analytical potential can reproduce the ab initio data used to fit its parameters and its contingent inability to reproduce some quantum effects that might happen in condensed phases. The approach with ab initio-based models has also been used to study aqeuous solutions of Na^+ and K^+ [86, 87], resulting in agreement with the QM/MM simulations of Refs. [73, 76], and of Li^+ [88], yielding agreement with the DFT-based molecular dynamics of Refs. [65, 68].

The parameters of polarizable models have also been fitted to reproduce simultaneously the experimental enthalpies of gas-phase monohydrates and the hydration free energies in the bulk liquid [89]. Besides the spread of experimental data for the hydration free energies [17, 90–94], this approach has the problem of finding the appropriate theoretical calculation of free energies [95–101].

The aim of this work is thus to generate a theoretical model for Rb^+–water interactions that can be used in classical numerical simulations, and can provide a reliable molecular picture of the relevant effects in Rb^+ hydration. In line with previous studies of lighter alkali metals [87, 88], the parameters of the analytical potential are fitted solely to reproduce single atom properties and high-quality ab initio calculations of small clusters.

2 Methods

2.1 Analytical model potentials

As in previous studies [87, 88] of Li^+, Na^+ and K^+, the MCDHO [83] analytical potential was used for the water–water interactions.

The water molecule is modeled with an effective positive charge Z_i on each nucleus i ($Z_O = +2.66e$, $Z_H = +0.62e$), and a negative charge density with a radial exponential decay, $\rho_M(r) = (q_M/\pi\lambda_M^3)\exp(-2r/\lambda_M)$ referred to as a shell (M), with its center attached to the oxygen atom with a harmonic spring k_M. The molecule is neutral, thus $\int\rho_M(r)\mathrm{d}\tau = q_M = -3.90e$. In addition to the electrostatic terms, the analytical intramolecular potential comprises Morse potentials for the O–H bonds,

$$U_b = D_{\mathrm{OH}}\left\{\exp\left[-2\gamma_{\mathrm{OH}}\left(r_{\mathrm{OH}} - r_{\mathrm{OH}}^{\mathrm{eq}}\right)\right] - \exp\left[-\gamma_{\mathrm{OH}}\left(r_{\mathrm{OH}} - r_{\mathrm{OH}}^{\mathrm{eq}}\right)\right]\right\},$$

and a quartic polynomial for the HOH bond angle,

$$U_\theta = a_{\mathrm{HOH}}\left(\theta_{\mathrm{HOH}} - \theta_{\mathrm{HOH}}^{\mathrm{eq}}\right) + b_{\mathrm{HOH}}\left(\theta_{\mathrm{HOH}} - \theta_{\mathrm{HOH}}^{\mathrm{eq}}\right)^2 + c_{\mathrm{HOH}}\left(\theta_{\mathrm{HOH}} - \theta_{\mathrm{HOH}}^{\mathrm{eq}}\right)^3 + d_{\mathrm{HOH}}\left(\theta_{\mathrm{HOH}} - \theta_{\mathrm{HOH}}^{\mathrm{eq}}\right)^4,$$

thus producing an intramolecular energy U_S.

For the intermolecular energy, the shells interact with the cores in other molecules with a different decay length λ_M', and with the other shells as point charges. Additional Lennard-Jones terms are added to the interaction between cores and shells in different molecules,

$$U_{ij} = \left(\frac{A_{ij}}{r_{ij}}\right)^{12} - \left(\frac{B_{ij}}{r_{ij}}\right)^{6},$$

where $r_{ij} = \|\mathbf{r}_i - \mathbf{r}_j\|$ is the distance between the corresponding sites. The sum of all interactions yields the energy U_N of a cluster with N molecules; subtraction of the intramolecular energies of the isolated molecules, U_S^0, yields the interaction energy $\Delta U_N = U_N - N \times U_S^0$. A more general description of the MCDHO-type model has been presented elsewhere [87, 102].

The same functional form had been used for the lighter alkali metals [87, 88]. In this case, the relatively weaker Rb^+–water interaction allowed some simplification: a point charge $q_{\mathrm{Rb}} = -2.0e$ could be used instead of a shell, whence the core charge was $Z_{\mathrm{Rb}} = +3.0e$. The experimental [17] polarizability $\alpha_{\mathrm{Rb}} = 1.62524$ Å^3 thus determined the harmonic spring force constant $k = 0.364709$ Hartree a_0^{-2} (1 Hartree = 627.51 kcal mol^{-1}, $a_0 = 0.52917726$ Å): the dipole induced by a weak electric field E is obtained from the displacement $\Delta r = qE/k$ of the charge, whence $\Delta\mu = q^2 E/k = \alpha E$.

Instead of the common 12-6 Lennard-Jones terms that were used for the smaller alkali metals, a sum of two exponentials

$$U_{\mathrm{Rb},i} = C_{\mathrm{Rb},i}\exp\left(-\frac{r_{\mathrm{Rb},i}}{s_{\mathrm{Rb},i}}\right) + C'_{\mathrm{Rb},i}\exp\left(-\frac{r_{\mathrm{Rb},i}}{s'_{\mathrm{Rb},i}}\right),$$

acting between the cores was found to produce a better fit to the ab initio pair interactions. A single exponential could have been used, but it yielded a slightly reduced quality of the fit; however, since the use of one or two exponential terms has an identical cost in the potential since it is tabulated, the two-term expression was used. The final parameters of the Rb^+–water intermolecular potential are shown in Table 1. They were fitted to reproduce ab initio calculations of interaction energies performed in this work with the strategy described in the next subsections.

2.2 Quantum calculations

The models, the parameters of which have been fitted to reproduce ab initio data are at most as accurate as the underlying quantum calculations. Thus, a level of the

Table 1 Parameters of the exponential terms for the Rb, O and Rb, H interactions

	C	s	C'	s'
Rb, O	599.609179	0.722630	−534.793796	0.7331174
Rb, H	1,671.373669	0.636208	−1,716.334083	0.633584

All quantities in atomic units: C and C' in Hartree, and s and s' in a_0

theory, as reliable as possible, has to be chosen, which can be extrapolated to condensed phases by means of numerical simulations, through the analytical model potential. The first task is to find the adequate level of theory to compute the sample points in the ab initio potential energy surfaces.

The Rb^+–(H_2O) interaction has been studied extensively with the ab initio method, using various different levels of the theory.

Glendening and Feller [103, 104] employed Dunning's [105] family of aug-cc-pVxZ (x = D, T, Q) basis functions for H and O, and the Hay and Wadt [106] relativistic ECP for the 1*s* through 3*d* electrons of Rb^+. The associated basis set for the valence electrons [107, 108] was augmented with additional diffuse and polarization functions to allow for a larger polarizability of the cation, resulting in $\alpha_{Rb} = 1.131$ Å^3. Their estimate of the complete basis set limit (CBS) yielded a dimerization enthalpy of $\Delta H = -14.7$ kcal mol^{-1}, which is 1.2 kcal mol^{-1} short of the experimental data [109], $\Delta H = -15.9$ kcal mol^{-1}.

Park et al. [110] also used the aug-cc-pVxZ family (that will be abbreviated as *a*VxZ henceforth) for H and O, but only with x = D, T. For Rb^+ they employed the Stuttgart relativistic small-core effective-core potential RSC97 ECP [111] and added a diffuse *d* function to the associated basis [107, 108] for the valence electrons, resulting in a better estimate of the polarizability, $\alpha_{Rb} = 1.267$ Å^3, and in enthalpies and free energies for $Rb^+(H_2O)_n$ clusters, in good agreement with experiment [109] for $n = 1, 2, \ldots, 5$. Thus, in this work it was decided to use the same ECP and basis set for Rb^+, with the *a*VQZ basis for H and O.

The Rb^+–(H_2O) dimer was optimized using the GAUSSIAN 03 code [112], which was employed in this work for all quantum calculations. The second-order many-body perturbation theory (MP2) [113] was used to account for the correlation energy. At first, no correction was made for the basis set superposition error (BSSE). The resulting interaction energies ΔE_e and r(Rb–O) distances are plotted in Fig. 1 as a function of the basis set size and compared to those obtained in Refs. [104, 110] (open symbols are used for uncorrected values). The progression x = D, T, Q in the *a*VxZ basis allows for estimates of the CBS limit, following the procedure described in Ref. [104], for various quantities: r(Rb–O) = 2.763 Å, $\Delta E_e = -20.8$ kcal mol^{-1}, and $\Delta H^{298} = -20.2$ kcal mol^{-1} (computed as in Ref. [110]). This latter value is exaggerated by 4.1 kcal mol^{-1}

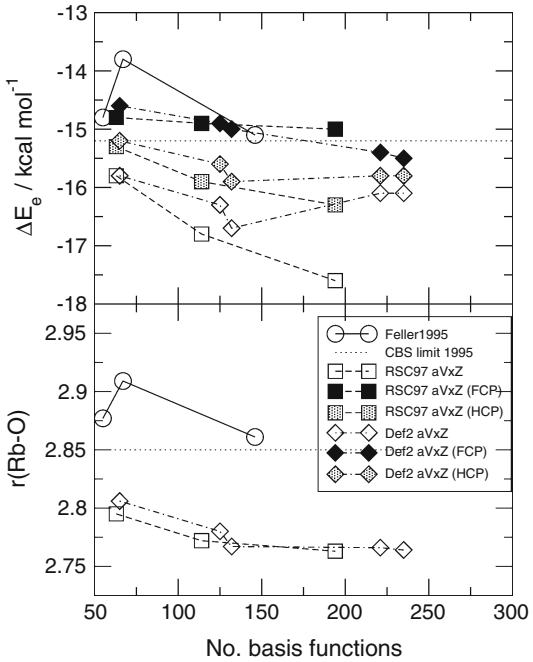

Fig. 1 Progression of the interaction energy ΔE_e (*top*) and the r(Rb–O) distance (*bottom*) predicted for the $Rb^+(H_2O)$ dimer with successively larger basis sets; DZ < 75 functions, 100 < TZ < 150 < QZ. Energies uncorrected for BSSE in *open symbols*; fully CP corrected in *black*, and half-corrected in *gray*

relative to the experiment. Such exaggeration can be ascribed to the BSSE, and thus the full counterpoise correction (FCP) [114] was applied. It resulted in a CBS limit for the interaction energy in agreement with that calculated without CP correction in Ref. [104] ($\Delta E_e = -15.2$ kcal mol^{-1}) (black symbols are used for FCP energies in Fig. 1), and in a theoretical $\Delta H^{298} = -14.4$ kcal mol^{-1}. It is thus unclear what value to use as the reference for the analytical model potential. The reliability of the ab initio method can be assessed by comparing the calculated enthalpy to the experimental data. However, as previously mentioned, the enthalpies computed by Park et al. [110] at the uncorrected MP2/*a*VTZ level were in good agreement with that of the experiment. It is clear from Fig. 1 that this agreement was fortuitous. The average of the MP2/*a*VQZ and the MP2/*a*VQZ(FCP) enthalpies found in this work also yielded good agreement with the experimental value: $\Delta H^{298}_{HCP} = (-17.0 - 14.4)/2 = -15.7$ kcal mol^{-1}. Therefore, the parameters of the ion–water potential were fitted to MP2/*a*VQZ(HCP) energies (HCP stands for *half-counterpoise*), which resulted in agreement of the hydration enthalpy with the experiment, as will be discussed in Sect. 3.2.6. It is to be noted that in a recent study of the water–water pair-interaction energies [115], a weighted average $\Delta E(w) = \Delta E + w\ (\Delta E(\text{FCP}) - \Delta E)$ between the uncorrected ΔE and the ΔE(FCP) values was made to reproduce the

benchmark of the dimerization energy and a value of $w = 0.52$ was found.

Nonetheless, it can be seen in Fig. 1 that for the series of RSC97 *a*VxZ energies the FCP values diverge from the uncorrected ones, so that the agreement might also be fortuitous. To better assess the reliability of the MP2/*a*VQZ(HCP) interaction energies, further calculations were performed with a more recent version of the Stuttgart ECP [116] and with the set of xZVP(P) basis sets for Rb^+ that were designed to be consistent with the *a*VxZ for H and O [117] (these sets are labelled as Def2 in [107, 108], and can be downloaded from http://bse.pnl.gov/bse/portal or from http://www.theochem.uni-stuttgart.de/pseudopotentials/clickpse.en.html under the name ECP28MDF). The results of these calculations are represented by diamonds in Fig. 1. It can be seen that at the MP2/*a*VQZ level, the optimal distance r(Rb–O) = 2.763 Å is the same as that of MP2/QZVP and MP2/QZVPP calculations. The BSSE of the corresponding interaction energies is consistently reduced, and the MP2/*a*VQZ(HCP) value, $\Delta E_e = -16.3$ kcal mol^{-1}, is close to the MP2/QZVPP result, $\Delta E_e = -16.1$ kcal mol^{-1}. An additional test of the validity of the MP2/*a*VQZ(HCP) approximation is discussed in the next section.

2.3 The fitting procedure

Quantum calculations at the MP2/*a*VQZ(HCP) level were performed with the GAUSSIAN 03 code [112] to generate a sample of 1971 Rb^+–H_2O pair interactions, which served to fit the parameters shown in Table 1. No further adjustment was made on the charges and spring constant of the Rb^+ cation.

The model was then compared to the sample of 1971 pair interaction energies, and to another set of 171 three-body and 62 four-body nonadditive contributions that were computed at the RHF/*a*VQZ(HCP) level for various $Rb^+(H_2O)_2$ and $Rb^+(H_2O)_3$ clusters, chosen at first from the optimal $Rb^+(H_2O)_n$ clusters, with $n = 2, 3,\ldots, 8$ (*vide infra*), and then from configurations found in preliminary simulations. The second-order many-body perturbation theory (MP2) [113] was used to account for the correlation energy solely for the pair interactions, because it is almost entirely additive [87, 118]. This first test of the ability of the model to reproduce the ab initio calculations can be seen from the quality of the adjustment to the ab initio values. The corresponding standard errors are: $e_{rms} = 0.51$ kcal mol^{-1} for the pair interactions, $e_{rms} = 0.19$ kcal mol^{-1} for the three-body nonadditive contributions, and $e_{rms} = 0.02$ kcal mol^{-1} for the four-body nonadditive contributions. It is worth to emphasize that only the total charge and the experimental polarizability of Rb^+, and the MP2/*a*VQZ(HCP) pair interactions were used in the parametrization.

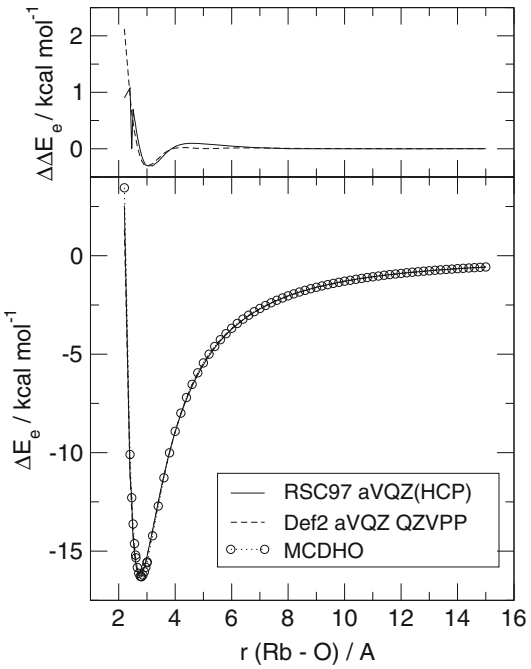

Fig. 2 Comparison of the pair interaction energies as a function of the r(Rb–O) distance, along the line of the optimal dimer. *Top* $\Delta\Delta E_e = \Delta E_e$ (MCDHO) − ΔE_e (ab initio). *Bottom* pair interaction energies

As mentioned in the previous section, a further comparison to MP2/QZVPP calculations is needed to ensure the exactness of the ab initio energies. This is done in Fig. 2, where the pair energies are plotted as a function of the r(Rb–O) distance, along the line of the optimal dimer. It is apparent that after 4 Å the difference between the model and either set of ab inito calculations is virtually null, which also corroborates the reliability of the MP2/*a*VQZ(HCP) energies. The larger positive differences of the model occur at distances shorter than 2.5 Å, and the negative ones occur around the minimum. This might produce a somewhat exaggerated height of the first peak in the radial distribution function (RDF) of the ion in aqueous solution.

The close agreement of the model with the ab initio energies beyond 4 Å was analyzed in Ref. [87], where it was shown that at a distance of approximately 3 Å, the ion–water interaction is almost completely that of a point charge with a dipole. A similar result had been reported in Ref. [119].

3 Results

3.1 Small clusters

To test the reliability of the models and their parametrization, their predictions of the interaction energy for various

different $Rb^+(H_2O)_n$ clusters were compared to ab initio calculations of stationary points with $n = 1, 2,\ldots, 8$ in Table 2. The geometries are represented in terms of the number of water molecules in the first and second hydration shells, n_1 and n_2, respectively, and they correspond to Fig. 1 of Ref. [110]. The ab initio results presented in this work and those of the classical models were compared to the best ab initio values of Ref. [110]. The configurations were optimized with the corresponding version of the MCDHO model in each case, whereas it was only possible to make full MP2/*a*VQZ optimizations for clusters with up to $n = 6$ water molecules; for $n = 7$ the MP2/*a*VDZ(HCP) level was used, and for $n = 8$ a single point MP2/*a*VDZ calculation was performed with the configuration optimized with the MCDHO flexible model (MCDHOff). The difference between the (flexible) MCDHO and the MP2/*a*VQZ values is less than 1.4 kcal mol^{-1} for $n = 1$–6; the larger discrepancies for $n = 7$, 8 correspond to MP2/*a*VDZ calculations and amount to about 3%. Moreover, the model was able to produce the same configurations as the ab initio stable local minima, albeit with somewhat different geometric parameters (distances and angles). The comparison was extended to calculations with the largest basis in this work, QZVPP + *a*VQZ, made for $n = 1$–4, for which the agreement with the flexible MCDHOff results is slightly improved. The effects of flexibility and polarizability can be judged from the results produced by the restricted versions of the model, a polarizable one that uses the average geometry of the water molecule in the liquid (rigid MCDHO = MCDHOr), and a nonpolarizable one with the same geometry and the mobile charge fixed at its average position in the liquid (nonpolarizable MCDHO = MCD) [102]. The total interaction energies are less negative, ca. 1 kcal mol^{-1} for MCDHOr and ca. 2 kcal mol^{-1} for MCD.

A further validation of the models can be made by comparing their predictions of the enthalpies ΔH^{298}_{hyd} of successively larger clusters at $T = 298$ K, to the theoretical [110] and experimental [109] data reported in literature. This was done by performing Monte Carlo simulations of the clusters and using the ideal-gas formula [120–122]

$$\Delta H = \Delta U + P\Delta V = \Delta U - nRT$$

where $P = 1$ atm is the pressure, n is the number of water molecules in the cluster, R is the gas constant, and $T = 298.15$ K the temperature. A correction of $\frac{3}{2}RT$ per molecule was added to correct for the classical sampling of the intramolecular degrees of freedom in MCDHOff. The results are presented in Table 3. The difference between the MCDHOff and the experimental values is less than 1 kcal mol^{-1} for $n = 1$–4 and increases to 1.7 kcal mol^{-1} (2.7%) for $n = 5$. The discrepancies of the MCDHOr and MCD results are slightly higher, mainly due to the

Table 2 Comparison of the total interaction energies (in kcal mol^{-1}) for stationary Rb^+–$(H_2O)_n$ clusters

n	Geometry	*a*VTZ (*a*VDZ)	*a*VQZ(HCP) (*a*VDZ(HCP))	QZVPP	MCDHOff	MCDHOr	MCD	SWM4-DP
1	1+0 (C_{2v})	−16.8	−16.3	−16.1	−16.2	−16.1	−15.5	−15.9
2	1+1 (C_s)	−29.8	−29.0	−29.2	−29.4	−29.0	−27.2	−27.8
	2+0 (C_2)	(−29.9)	−31.0	−30.6	−30.6	−30.2	−28.7	−30.2
	2+0 (C_s)	−31.9		−30.6	−30.6			−30.2
	2+0 (D_{2d})	(−29.6)	−30.1	−30.3	−30.4[a]	−29.6[a]	−29.7[a]	
3	2+1 (C_{2v})	−47.4	−45.9	−45.8	−45.3	−44.7	−42.6	−44.1
	3+0 (C_3)	−47.4	−45.8	−45.7	−43.2	−42.5	−39.2	
	3+0 (D_3)	−45.6	−44.2	−43.4	−43.3	−42.6	−41.5	−43.2
4	3+1 (C_1)	−60.2	−56.6		−57.2	−56.3	−54.7	−56.4
	4+0 (C_4)	−62.9	−59.1	−61.4	−58.0	−57.3	−55.2	
	4+0 (S_4)	(−53.8)	−53.9		−54.6	−53.4	−50.9	−54.8
5	4+1*h* (C_1)	(−73.8)	−72.6		−71.3	−70.4	−68.0	
	5+0 (C_2)	(−71.9)	−71.0		−69.7	−68.7	−67.2	
6	4+2*h* (C_2)	(−87.2)	−85.2		−83.9	−82.7	−80.6	−80.4
	5+1*h* (C_1)	(−85.1)	−83.6		−82.3	−81.0	−78.9	
7	5+2*h* (C_1)	(−97.5)	(−92.1)		−94.1	−92.5	−89.7	
	4+3*h* (C_1)		(−94.4)		−96.7	−95.7	−93.2	
8	8+0 (C_4)	(−110.7)	(−103.7[b])		−105.6	−103.9	−101.5	

All quantum calculations include the correlation energy at the MP2 level. *a*VDZ and *a*VTZ from Ref. [110]. SWM4-DP from Ref. [89]

[a] Oxygen positions fixed

[b] Single-point calculation on the MCDHO optimized geometry

Table 3 Comparison to experimental data [109] (HPMS: high-pressure mass spectrometry) and to theoretical ab initio estimates (*a*VTZ from Ref. [110]) of the cumulative enthalpies (in kcal mol^{-1}) produced by the model in gas-phase simulations for Rb^+–$(H_2O)_n$ clusters at $T = 298.15$ K, as described in the text

n	HPMS	*a*VTZ	MCDHOff	MCDHOr	MCD
1	−15.9	−16.2	−16.0	−15.8	−15.1
2	−29.5	−29.9	−29.8	−29.4	−28.6
3	−41.7	−42.1	−41.7	−41.0	−39.5
4	−52.9	−53.4	−52.2	−50.9	−48.8
5	−63.4		−61.7	−60.4	−57.8

restraints imposed on the molecular geometry of both versions and on the dipole moment of MCD.

For a more refined analysis, the enthalpies of the detachment reactions

$$Rb^+(H_2O)_n \rightarrow Rb^+(H_2O)_{n-1} + H_2O$$

are plotted in Fig. 3. For $n = 1$ and 2, the models' values were somewhat higher than the experimental data, but after $n = 3$ the situation was reversed. The largest deviation from the experiment occurs for MCD.

The relatively weak Rb^+–water interactions lead to structures where the stability is mostly due to the formation of hydrogen bonds among water molecules (Fig. 4). This behavior is reproduced by the three versions of the model.

The previous comparison led to the conclusion that the three versions of the MCDHO model were suitable for numerical simulations of the aqueous solution under ambient conditions.

3.2 Aqueous solution

3.2.1 Numerical simulations

The insertion of Rb^+ in an equilibrated system of liquid water required the removal of five water molecules (the partial molar volume is positive and large [17], $V^{\infty}(Rb^+, aq) = 8.6\,cm^3\,mol^{-1}$) and a subsequent relaxation of its size to avoid spurious effects from short-range repulsion. Thus, a first set of Monte Carlo simulations with the Metropolis algorithm [123, 124] was performed on the isothermal–isobaric *NPT* ensemble at $T = 298.15$ K and $P = 1$ atm, for a system of 995 water molecules and one Rb^+ ion in a cubic cell. The intramolecular vibrations were sampled classically for MCDHOff; single update of the polarization was used. A spherical cutoff radius of $R_c = 15.35$ Å was used for the intermolecular interactions, as well as periodic boundary conditions with Ewald sums [125], to account for long-range electrostatics. The resulting average box length, $\langle L \rangle = 30.85$ Å (with a density $\langle \rho \rangle = 1{,}014$ kg m^{-3}), was then used in three simulations of the same system on the

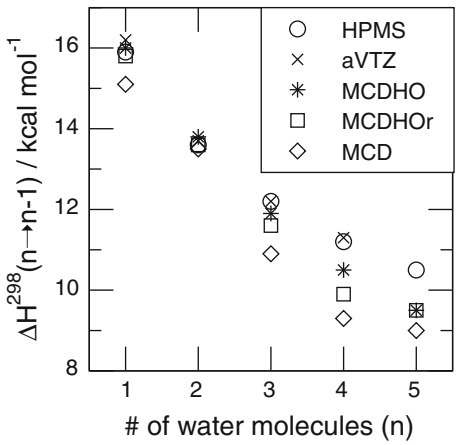

Fig. 3 Enthalpies of the detachment reactions $Rb^+(H_2O)_n \rightarrow Rb^+(H_2O)_{n-1} + H_2O$, $n = 1, 2,\ldots, 5$, in kcal mol^{-1}. *HPMS* high-pressure mass spectrometry [109]. *aVTZ* from Ref. [110]

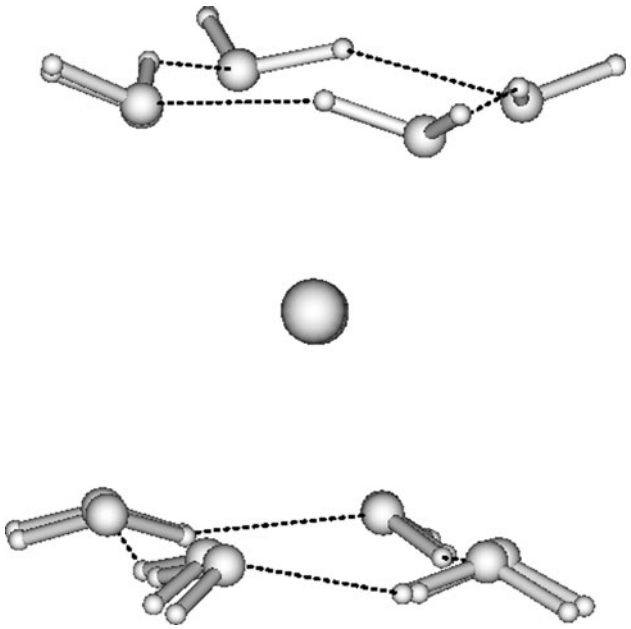

Fig. 4 Superposition of the optimal $Rb^+(H_2O)_8$ cluster found with the model on the ab initio optimum. The eight water molecules surrounding the Rb^+ ion arrange as two separate water tetramers

canonical *NVT* ensemble, one with each of the three versions of the MCDHO model. In all cases, the rubidium ion was considered polarizable.

3.2.2 Structure

Because the Rb^+–water interaction is relatively weak, the water molecules in its surroundings can assume a wide range of hydration distances [15, 19, 33]; however, a well-defined hydration shell has been found even at high temperatures [22, 24] and pressures [29]. The partial radial

distribution functions (rdf's) $g_{\mathrm{RbO}}(r)$ and $g_{\mathrm{RbH}}(r)$ have been deduced from neutron and X-ray diffraction structure factors [33, 34], through a combined molecular dynamics (MD) and reverse Monte Carlo (RMC) approach [62, 63], with a rigid, nonpolarizable model potential. The reverse Monte Carlo technique involves refining a starting interatomic potential energy function in a way that produces the best possible agreement between the simulated and measured site-site partial structure factors [126]. But to be successful, the rdf's must uniquely determine the higher order correlation functions. This, in turn, can only occur in a pairwise additive system [126, 127].

The rdf's resulting from the simulations in this work are shown in Fig. 5, and compared to the data derived from those experiments. While the agreement is very good for the first peak of $g_{\mathrm{RbO}}(r)$, the models fail to reproduce the depth of the first minimum. For the three models the first maximum is located at 2.9 Å, in agreement with the experimental data [19, 24, 26, 28–30, 32], which range from 2.83 to 3.05 Å and depend on the concentration. The figure from previous classical simulations [54, 55, 61–63, 119] ranges from 2.9 to 3.15 Å, and from QM/MM [74] is 2.95 Å. In agreement with the experimental data, the models predict two more maxima for $g_{\mathrm{RbO}}(r)$, but shifted to about 0.2 Å for shorter distances and narrower by the same amount. Though the correctness of the rdfs deduced from experimental data is debatable, these discrepancies cast some doubt on the correctness of the theoretical results found in this work about the second and third hydration shells. A simulation of the RbBr solution would be needed to validate the models by direct comparison to the measured structure factors; but this goes beyond the aims of the present work.

On the other hand, the agreement with experiment is better for the simulated $g_{\mathrm{RbH}}(r)$, with exception made of the height of the first maximum. A possible explanation of this behavior is that classical simulations with ab initio-based models do not take into account the quantum delocalization of the proton, which affects both the interactions and the structure of aqueous solutions [128–130]. The size of the effects is proportional to the reduced mass m between the proton and the atom with which it interacts [131–133], thus larger for the Rb^{+}–H interaction than for the O–H. Of course, to fully test the possible effect on $g_{\mathrm{RbH}}(r)$, a path-integral method would be required, but a coarse approximation suffices to show the general trend. In this case, the classical rdf was deconvoluted with a Gaussian packet [131]:

$$g^{q}_{\mathrm{RbO}}(r) \approx \left(\frac{6m}{\pi\hbar^2\beta}\right)^{1/2}\frac{1}{r}\int_0^\infty u g_{\mathrm{RbO}}(u) \times \left\{\mathrm{e}^{-6m(r-u)^2/\beta\hbar^2} - \mathrm{e}^{-6m(r+u)^2/\beta\hbar^2}\right\}\mathrm{d}u,$$

where $\hbar$ is Planck's constant, k_B is Boltzmann's constant, and $\beta = 1/k_B\,T$. The resulting $g^{q}_{\mathrm{RbO}}(r)$ is compared to the classical and to the experimental $g_{\mathrm{RbO}}(r)$ in the inset of Fig. 5. As expected, a better agreement with experiment was attained. This result suggests the possible need to take into account the delocalization of the proton in all ab inito-based simulations.

Thus, the RbO rdf's resulting from the simulations in this work show three hydration shells: the first one up to 3.6 Å; the second one up to 5.6 Å, and the third one up to 8.1 Å. These values define the three hydration shells that

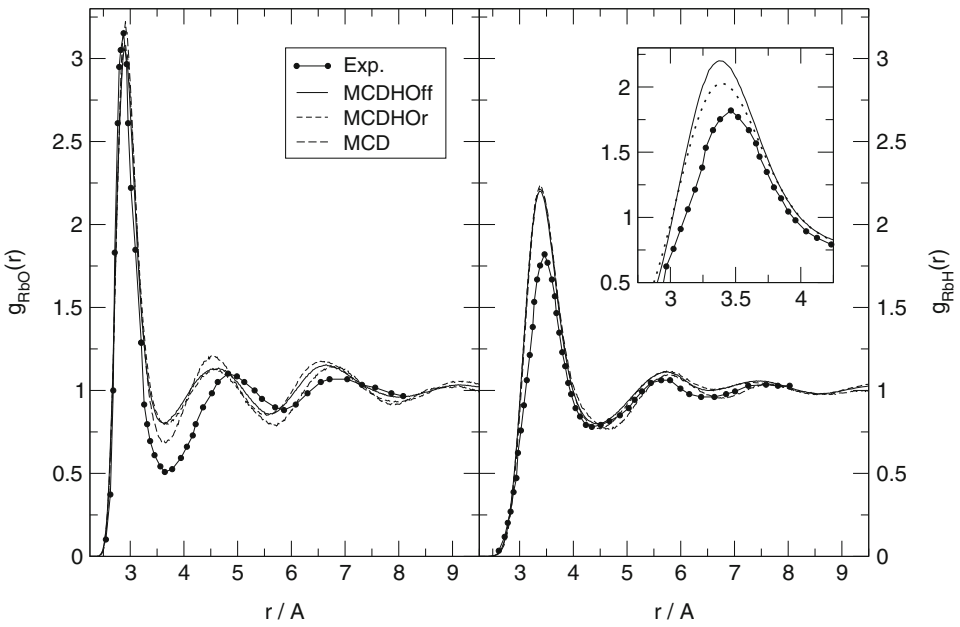

Fig. 5 Comparison to experimental data of the radial distribution functions produced by the models. *Inset* the *dotted line* includes an approximate correction to account for the delocalization of the H atom (see Ref. [131])

will be discussed in the next subsections and are subject to the inaccuracies mentioned in the previous paragraphs.

3.2.3 Coordination

The coordination number (CN) derived from different experimental techniques for Rb^+ ranges from 6 to 8 [18, 19, 22, 24, 26, 28, 30], with a most likely value of CN = 6.9 at low concentration [26, 27, 32, 34]. The CN can be obtained from a simulation by integrating $g_{RbO}(r)$, or by computing the distribution of the number of Rb^+–O neighbors at distances up to the first minimum of $g_{RbO}(r)$ (Fig. 6). The results in this work were CN = 6.84 for MCDHOff and MCD, and CN = 6.93 for MCDHOr. Early simulations with empirical model potentials [54–59] reported CN to be between 8 and 9; the same result was obtained by fitting the Rb^+–water interaction to ab initio calculations, with a nonpolarizable water model [119], and from fitting the gas-phase monohydrate and the hydration free energy in bulk water with polarizable models [89]. More recent quantum calculations of isolated hydrates [134] yielded CN = 6; QM/MM molecular dynamics [74] predicted CN = 7.1, and recent simulations with model potentials parametrized through reverse Monte Carlo [62, 63] produced a lower value, CN = 5.52. The CN distributions in this work are narrower than those reported in Ref. [63] and very similar to those in Ref. [74], though with a maximum at CN = 7, instead of 8, and skewed to the left, instead of to the right.

3.2.4 Effects of the ion on the structure of water

The main effect to be expected from an ion is the alignment of the water dipole to the ion's electric field; but it has been shown from neutron diffraction data [135] and simulations of lighter alkali metal ions [87, 88] that the average angle ϕ between the water dipole and the ion's electric field is not null. The distributions over the sphere of ϕ for the three models used in this work are depicted in Fig. 7, for molecules in the three previously mentioned hydration shells and in bulk (i.e., for Rb^+–water distances longer than 8.1 Å). The distribution of an angle over the sphere is weighed by its corresponding area on the surface. For the first shell, the three models produce asymmetric distributions, with maxima at $\phi = 54°$, MCDHOff and MCDHOr, and at $\phi = 51°$ for MCD. A more dramatic difference of MCD was found for the second and third shells; both polarizable models produced such a damping of the ion's field, that the corresponding distributions of ϕ become rather flat, whereas the nonpolarizable model keeps a more

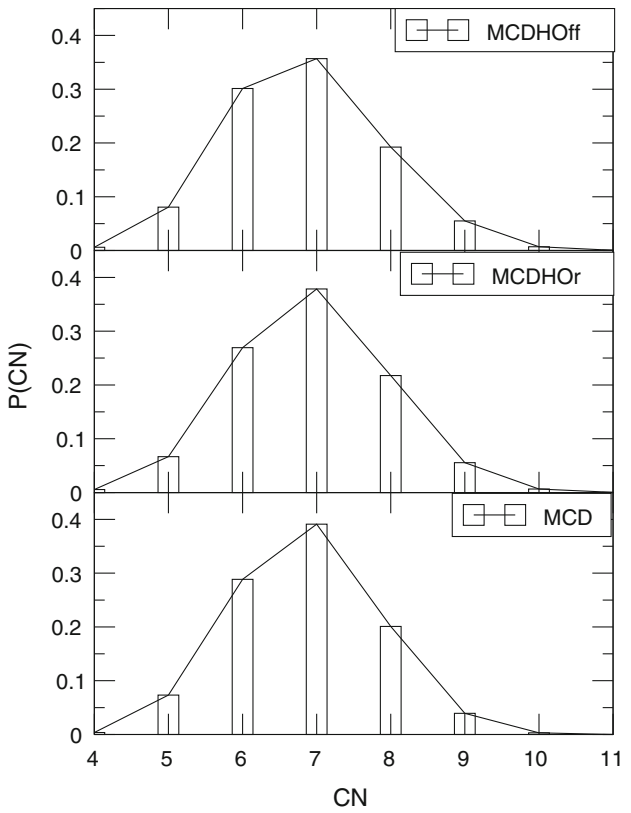

Fig. 6 Distributions of the number of water molecules in the first hydration shell of Rb^+

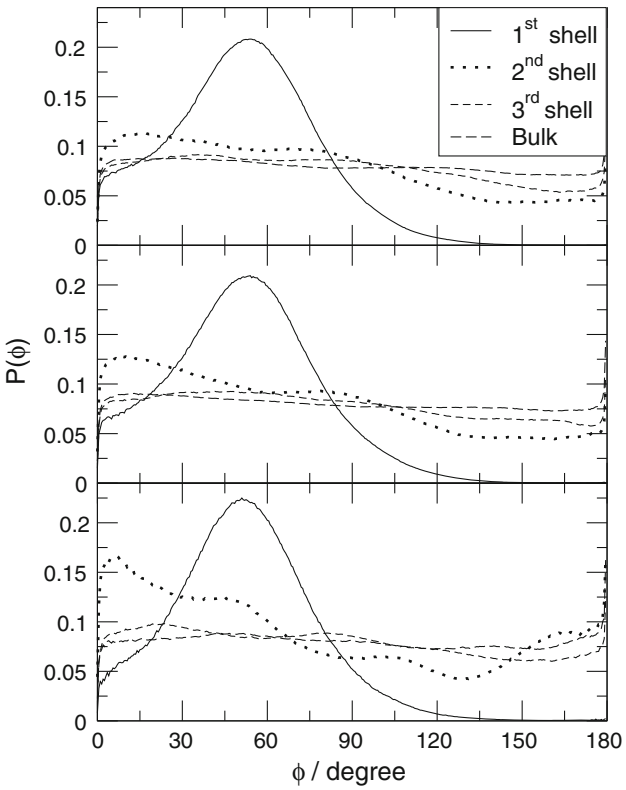

Fig. 7 Distributions of the angle ϕ between the water dipole and the ion's electric field. *Top* MCDHOff. *Middle* MCDHOr. *Bottom* MCD

significant alignment. The three models show uniform distributions for bulk water molecules.

3.2.5 *Effect of the ion's electric field on individual water molecules*

To analyze the effect of the ion's electric field on the individual water molecules, the per-molecule dipole moment was computed at each region for MCDHOff and MCDHOr. The corresponding distributions are presented in Fig. 8. The bulk value was obtained from simulations of liquid water under the same conditions described above (Sect. 3.2.1), resulting in $\langle \mu(H_2O) \rangle = 3.02$ and 2.97 Debye, for MCDHOff and MCDHOr, respectively. In contrast to the case of Li^+ [88], a lower dipole was found for the water molecules in the first hydration shell with both polarizable models, $\langle \mu(H_2O) \rangle = 2.92$ and 2.89 Debye. The bulk value was recovered from the second shell onward. A similar result was found for K^+ by Whitfield et al. [67], whereas in previous simulations of Na^+ and K^+ with MCDHOff, the same dipole was found in all hydration shells and the bulk [87]. The reduction of the water dipole in the first shell, compared to liquid water, can be understood in the following terms. The lack of orientation toward the ion, which would induce a larger dipole, and also a lack of hydrogen bonding, responsible for increased dipole in liquid water, with the second shell water molecules were produced by the clathrate-like structure.

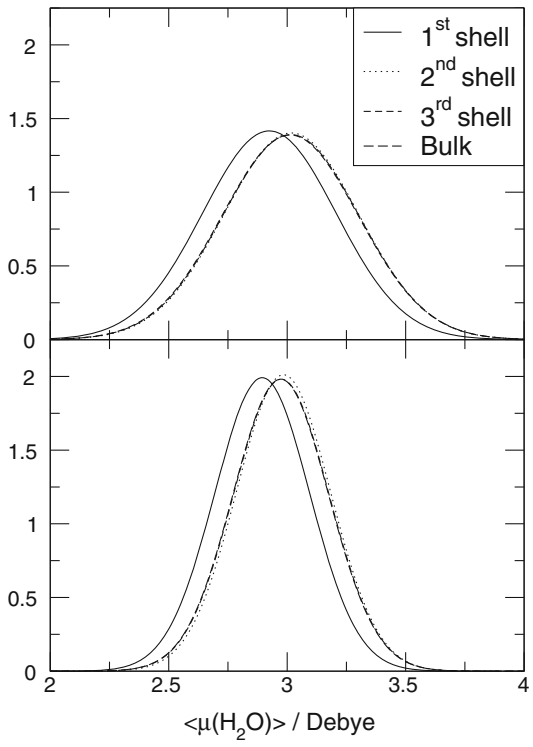

Fig. 8 Distributions of the per-molecule dipole moments. *Top* MCDHOff. *Bottom* MCDHOr

The effect of the ion's field on the intramolecular geometry was even lower. The distribution of the r(O–H) bond length and the $\widehat{HOH}$ angle of the water molecules in the first, second and third hydration shells are very similar to those of bulk water molecules, and the same applies to the two bond lengths of the water molecule. This negligible effect on the geometric properties of the water molecules explains the good performance of the rigid $MCDHO_r$ model. Though noticeable, the effect on the polarization is a mere 4%, thus the MCD model performs reasonably well.

3.2.6 *Thermodynamics*

The experimentally determined hydration enthalpy $\Delta H_{hyd}[Rb^+]$ should provide a benchmark to validate the results from the simulations. However, the experimental estimates of the hydration enthalpies of individual ions may vary by as much as 15 kcal mol^{-1} from one another, because they depend on the partition scheme used to distribute the hydration enthalpy of the salt among the resulting solvated ions [136, 137]. The estimates from experimental data are mainly affected by the value of the absolute hydration enthalpy of the proton, $\Delta_{hyd}\, H°[H^+]$ used as a reference: The quantity that can be determined from direct experimental measurements is the enthalpy to place a pair of oppositely charged, gas phase ions into water at 298 K, $\Delta_{hyd}\, H[XY]$, which is obtained in most cases from the difference of the standard heat of solution and lattice energy for the corresponding electrolyte [91]. The average differences between two cations, X_1^{z+} and X_2^{z+}, in salts with the same anions can then be used to assign the conventional hydration enthalpies, $\Delta_{hyd}\, H^{\circ}_{conv}[X^{z+}]$; the absolute enthalpies can be calculated from the conventional ones if the absolute hydration enthalpy of at least one cation is known. Though there has been an attempt to use Na^+ as a Ref. [91], most compilations refer to the proton, thus

$$\Delta_{hyd}\, H°[X^{z+}] = \Delta_{hyd}\, H^{\circ}_{conv}[X^{z+}] + z\Delta_{hyd}\, H°[H^+].$$

Several experimental approaches to determine $\Delta_{hyd}\, H°[H^+]$ have been reported, the most recent of which are:

1. The tetraphenylarsonium-tetraphenylborate (TATB) extrathermodynamic assumption [17, 90] that $\Delta_{hyd}\, H°[(C_6H_5)_4As^+] = \Delta_{hyd}\, H°[(C_6H_5)_4B^-]$, resulting in $\Delta_{hyd}\, H°[H^+] = -261.5$ kcal mol^{-1}.
2. The "cluster pair-based approximation" [91, 92, 94] that is good for a specific pair of oppositely charged ions. This consideration assumes that plots of the cluster pair-based approximation for the proton solvation enthalpy versus cluster solvation enthalpy

difference for the various pairs of oppositely charged ions at specific cluster sizes will intersect at the true value (i.e., a common point) where the approximation is best. This leads to $\Delta_{\rm hyd}\ H°[{\rm H}^+] = -274.9$ kcal mol^{-1}.

3. The "enthalpy–entropy compensation" [93], based on the thermodynamics of the dissociation of water, which results in an entropy of $S°[{\rm H}^+_{\rm aq}] = -1.3$ cal K^{-1} mol^{-1} and an absolute hydration enthalpy of $\Delta_{\rm hyd}\ H°[{\rm H}^+] = -257.6$ kcal mol^{-1}.

In a recent work, Warren and Patel [101] favor the cluster-pair assumption and claim that on correcting the standard states, the free energies reported under the TATB assumption by Marcus [17, 90] are in agreement (within $\sim$2 kcal mol^{-1}) with those by Kelly et al. [94]. Moreover, the quantum calculations by Zhan and Dixon [138] of the hydration free energy of the proton also agree within 2 kcal mol^{-1} with the result from the cluster-pair assumption. Thus, the value deduced from the cluster-pair assumption for the hydration enthalpy for Rb^+ is [92, 94, 139, 140] $\Delta H_{\rm hyd}[{\rm Rb}^+] = -85.0$ kcal mol^{-1}, whereas that reported by Marcus [17, 90] is $\Delta H_{\rm hyd}[{\rm Rb}^+] = -72.9$ kcal mol^{-1}, and the consideration of the enthalpy–entropy compensation leads to [93] $\Delta H_{\rm hyd}[{\rm Rb}^+] = -67.6$ kcal mol^{-1}.

As it was done previously [87, 88] for the lighter alkali metals, an estimate of $\Delta H_{\rm hyd}[{\rm Rb}^+]$ was obtained in this work from the difference between the average of the total interaction energy of the system $\langle E_S\rangle$ and n times the average energy of a single water molecule, $\langle E_{\rm H_2O}\rangle$, i.e.,

$$\triangle_{\rm hyd}E = \langle E_S\rangle - n\langle E_{\rm H_2O}\rangle,$$

where n = 995 is the number of water molecules in the system. The effect of constant pressure was taken into account indirectly as described in Sect. 3.2.1. The blocking method of Flyvbjerg and Petersen [141] was used in all cases to make sure that convergence was attained and statistical sampling was significant. The resulting hydration energies were $\Delta_{\rm hyd}\ E[{\rm Rb}^+] = -61.0$, -58.6 and -61.1 kcal mol^{-1} for MCDHOff, MCHDOr and MCD, respectively. The same value was obtained previously [119] with model potentials that were also fitted to counterpoise corrected ab initio calculations. That hydration energy corresponds to a 10% underestimation with regard to the lowest reported experimental hydration enthalpy, and in that work such underestimation was ascribed to the overcorrection of the pair interaction energy resulting from applying the full counterpoise method. However, in this work, the comparison to the experimental enthalpies of gas-phase clusters (Table 3) validated the interaction energies predicted by the MCDHO models. Thus, the comparison to experimental data requires taking into account the finite-size limitations of the simulation methods. The most significant correction to be added is ΔH_{ϕ_W}, to remove the ion–ion self-potential due to Coulombic interactions between the ion and its periodic replicas, which appear when Ewald sums are used with a neutralizing background charge density and tinfoil boundary conditions [95], i.e., the Wigner potential ϕ_W of the ion. The correction depends on the ionic charge z, on the box length L and on the electric permittivity of the solvent, ε_S and that of vacuum ε_0; thus

$$\Delta H_{\phi_W} = \frac{z^2}{8\pi\varepsilon_0}\left(1 - \frac{1}{\varepsilon_S}\right)\frac{\xi_{Ew}}{L},$$

where $\xi_{Ew} = -2.837297$ [95, 97, 98, 100]. Strictly speaking, the correction should include the change in box length when sampling the isobaric–isothermal ensemble [101]. Instead, the NVT ensemble was used in this work. For MCDHO water $\varepsilon_S = 110$ [102], thus in this work $\Delta H_{\phi_W} = -15.2$ kcal mol^{-1}, whence the resulting hydration enthalpies of Rb^+ turn out to be $\Delta_{\rm hyd}\ H[{\rm Rb}^+] = -76.5$, -74.1 and -76.6 kcal mol^{-1}, values that lie between those derived from the cluster-pair and the TATB assumptions.

Various other different corrections have been proposed in the last decade [95–100], and a recent revision can be found in Ref. [101], where five contributions to the real free energy of hydration are added to those derived from standard thermodynamic integration (TI) [142]:

$$\Delta_{\rm hyd}\ G_{\rm real} = \Delta_{\rm hyd}\ G_{TI} + \Delta G_{\phi_W} + \Delta G_{\varepsilon} + \Delta G_{\kappa} + \Delta G_{\rm LRC} + \Delta G_{\phi_\mu+\phi_Q}.$$

The term $\Delta G_{\phi W}$ corresponds to the Wigner potential mentioned in the previous paragraph, whereas the term ΔG_{ε} is necessary to correct for inappropriate polarization of the solvent within the unit cell [96, 99–101] and depends on the ionic radius R_I:

$$\Delta G_{\varepsilon} = \frac{z^2}{6\varepsilon_0 L}\left(1 - \frac{1}{\varepsilon_S}\right)\left[\left(\frac{R_I}{L}\right)^2 - \left(\frac{R_I}{L}\right)^5\right].$$

In this case $(R_I/L) \approx 0.08$, thus $\Delta G_{\varepsilon} = 0.14$ kcal mol^{-1}.

The finite volume correction ΔG_{κ} corresponds to the mean of the Ewald potential [98, 101] and depends on the screening charge parameter κ:

$$\Delta G_{\kappa} = -\frac{z^2}{8\varepsilon_0\,\kappa^2\,L^3},$$

which in this work turns out to be $\Delta G_{\kappa} = -0.3$ kcal mol^{-1}.

The long range correction $\Delta G_{\rm LRC}$ was neglected in this work because a large cutoff radius was employed.

Finally, the term $\Delta G_{\phi_\mu+\phi_Q}$ is added to take into account the interfacial potential jump resulting from the orientational disorder of the molecules at the air–water boundary [89–101]; the potential can be divided into a dipolar ϕ_μ and

a quadrupolar ϕ_Q contributions. An assessment of ϕ_μ would require a simulation of a water slab [68, 101] that has not been done for the MCDHO model, whereas ϕ_Q can be computed from the quadrupole trace $\gamma = \sum_i^{Ns} Z_i r_i^2$ of orientationally disordered solvent molecules, where *Ns* is the total number of interacting sites in the molecular model, Z_i is the respective (core) charge, and r_i is the respective distance to the center of the shell (in the MCDHO water model), whence $\phi_Q = -27.72$ kcal mol^{-1} e^{-1}. The reported dipolar contribution found for a number of water models ranges from 13.5 to 17.0 kcal mol^{-1} e^{-1} [99–101], therefore the total potential jump of MCDHO can be expected to lie between -14.2 and -10.7 kcal mol^{-1} e^{-1}, in agreement with the values obtained for other water models [68, 89]. Upon applying these additional corrections to the results of this work, the hydration enthalpies of Rb^+ attain values between -90.8 and -85 kcal mol^{-1}, closer to that from the cluster-pair assumption.

In line with Ref. [87], a further analysis was made of the interaction energies between the ion and the water molecules in the different shells and the bulk for MCDHOff (Table 4). Obviously, this partition of energies cannot take into account the contributions from the reciprocal space and the screening of charges used for the Ewald sums. Thus, the hydration energy $\Delta_{hyd}E^*$ [Rb^+] to be used as a reference was obtained by re-calculating without the Ewald method, from the simulations already performed, the average energy $\langle E_S^* \rangle$ of the aqueous solution and the *total* energy $\langle E_{liq} \rangle$ of the system of 995 water molecules without the Rb^+ ion. The reference hydration energy was obtained from the difference $\langle E_S^* \rangle - \langle E_{liq} \rangle$ and turned out to be $\Delta_{hyd}E^*$ [Rb^+] $= -83.2$ kcal mol^{-1}.

Table 4 Average interaction energy (kcal mol^{-1}) of the cation Rb^+ or a water molecule in a specific hydration shell W_i (columns), with the cation Rb^+ and with all the water molecules in W_j (rows), where i, $j = 1, 2, 3$ or b (bulk)

$\langle n \rangle$	Rb^+ 1	W_1 6.84	W_2 17.90	W_3 52.75	W_b 917.51
W_1	−39.56	0.03	−3.22	−0.33	−0.01
W_2	−16.43	−7.83	−4.44	−2.51	−0.04
W_3	−11.03	−2.45	−7.74	−7.31	−0.46
W_b	−9.05	−0.73	−1.99	−7.94	−17.79
W	−76.06	−10.98	−17.40	−18.09	−18.29
δ	0.08	6.58	7.60	7.66	7.68
Rb^+	0.00	−5.68	−0.96	−0.21	−0.01
Total	−75.98	−10.08	−10.75	−10.63	−10.62

(W_i,W_j) ≠ (W_j,W_i) because the number of molecules $\langle n \rangle$ is different in each layer.The sum of the corresponding column yields the interaction with all the water molecules in the system (W). Total includes the energetic cost δ of polarizing and deforming the molecule relative to the gas-phase polarization and geometry as well as the interaction with Rb^+

Table 5 Contributions to the hydration energy ΔE_{hyd} (kcal mol^{-1}) from the three hydration shells, obtained by subtracting the total for W_b from the total for W_i in Table 4, and multiplying by the number of water molecules in i

	Rb^+	K^+
W_1	3.70	1.78
W_2	−2.33	1.32
W_3	0.53	−3.97
(X^+, W)	−75.98	−75.96
ΔE_{hyd}	−74.08	−76.83

The results for K^+ are taken from Ref. [87]

The energetic cost δ of polarizing and deforming the molecule relative to the gas-phase polarization and geometry was considered separately from the other contributions to the energy. The results for Rb^+ turned out almost equal to those reported for K^+ in Ref. [87] (Table 5). The total interaction of the ion with water is distributed as follows: 52% with the water molecules in the first hydration shell, 21.6% with those in the second hydration shell, 14.5% with the third-shell molecules, and 11.9% with the bulk (for a comparison, it has to be noted that in Ref. [87], δ was included in the corresponding interaction and the energies were displayed horizontally). For first-shell water molecules, the interaction with the ion pays for 86% of δ. A similar analysis was performed in Ref. [55], where the SPC/E water model [143] was used with the nonadditive ion–water potentials of Liem X. Dang [120]; the reported Rb^+–water interaction is almost twice as much as found here, the same as their results for Na^+ and K^+ compared to Ref. [87]. Though in Ref. [55] no specific calculation is made of the hydration enthalpy, their reported ion–water interaction energies suggest a gross overestimation.

4 Concluding remarks

For this study, a Rb^+–H_2O analytical potential was fitted to ab initio calculations and to the experimentally determined polarizability of the ion. In the process, a new assessment of the *correct* ab initio Rb^+–water interaction was obtained, through the use of successively larger basis sets, which allowed a new determination of the CBS limit. It was also found that the adequate procedure for correcting the BSSE with the smaller basis involved the average of uncorrected and fully CP corrected energies, in agreement with other studies [115].

Care was taken in this work to validate the interaction energies produced by the models by comparing them to high-quality ab initio calculations of small clusters

(Table 3) and to the corresponding experimentally determined enthalpies (Table 3). Moreover, it can be seen in Table 2 that the MCDHO energies also agree with those of Lamoureux and Roux [89] who attempted to fit simultaneously the experimental enthalpies of gas-phase monohydrates and the hydration free energies in the bulk liquid.

The Rb^+-H_2O analytical potential was employed with three versions of the MCDHO model for water [83, 102] in numerical simulations of the diluted aqueous solution under ambient conditions. Validation of the simulation was done by comparing with the experimental thermodynamic and structural data. There is agreement with the first peak of the RbO rdf, but not with the second one. This could be taken as an indication of weakness of the potential, in spite of the agreement mentioned previously, or a dependency of the experimental curve on the potential used in the RMC method. The raw hydration enthalpy obtained from the simulation and the values obtained, when the corrections proposed in literature [95–101] were applied, fell within the range of the experimental values [17, 90, 92–94, 139, 140].

With regard to the coordination number (CN) of Li^+, there is consensus with different theoretical approaches [65, 68, 69, 88] that $CN(Li^+) = 4$. On the other hand, there is still a debate concerning Na^+ and K^+. Results from DFT-based calculations of ion-water clusters [134] and molecular dynamics simulations of aqueous solutions [66, 69] led to conclude that $CN(K^+) = CN(Na^+) = 4$; but, as mentioned in the introduction, this conclusion has been criticized as a possible artifact due to the inability of density functionals to properly describe hydrogen-bonded liquids [70, 71]. On the other hand, the results from QM/MM [73] and QMCF [76] simulations are $CN(Na^+) = 5.5$ and $CN(K^+) = 6.8$, with a broad distribution for this latter ion. The discrepancy was ascribed to the lack of correlation energy in these simulations [69]. However, further DFT-based simulations [67] of the aqueous solution of K^+ arrived at values for $CN(K^+)$ between 5.9 and 6.6, with broad distributions. The figure obtained from simulations with an empirical polarizable model [67] is between 6.5 and 6.8 for K^+, whereas from simulations with ab initio-based polarizable models [87], $CN(K^+) = 7.8$ and $CN(Na^+) = 5.6$. In the case of Rb^+, the results in this work show a clear convergence with other sophisticated theoretical methods [74] that predict a hydration number of seven, which is the value determined from experiments in diluted solutions [26, 27, 32, 34].

The analysis of the energies in Table 5 showed an enhancement of the water–water interactions in the second hydration shell relative to the bulk, somewhat different from the findings for K^+ in Ref. [87], where the enhancement was found to occur at the third hydration shell. Apart from that, the energy partition turned out to be very similar to that of K^+, as well as the overall structure deduced from $g_{RbO}(r)$ and $g_{RbH}(r)$. These similarities can be explained by the fact that at distances longer than 3 Å the monocation–water interaction is dominated by the point charge-(enhanced) dipole term [87, 119]. This fact can also explain why the first hydration shells [32] of K^+, Rb^+ and Cs^+ are all located at *ca.* 3 Å. This seems incongruous with the observed stepwise hydration of Rb^+ where the ion field does not command the arrangement of the water molecules in the clusters, opposite to K^+. However, when the complete solute is considered, the energetic advantage of alignment to the ion's field is superseded by that of forming a hydrogen-bonded network in the first hydration shell.

Thus, the results suggest that the hydrated cations of group IA can be divided into: hydrated Li^+, with $CN = 4$ in a rigid tetrahedron; hydrated Na^+, with $CN = 6$ in a rigid octahedron; and the rest, with a broad distribution of the number of water molecules in the first hydration shell, and an average $\langle CN \rangle \sim 7$.

Acknowledgments The financial support by CONACyT (Grant No. I-49396) and DGAPA-UNAM (Grant No. IN111706) is acknowledged. Part of the calculations was performed in the Kan Balaam supercomputer at DGSCA-UNAM. Iván Ortega-Blake *On leave from: Instituto de Ciencias Físicas, Universidad Nacional Autónoma de México, Apartado Postal 48-3, 62251 Cuernavaca, Morelos, México.*

References

1. Ritter SK (2003) Chem Eng News 81(36):27
2. Van Rysselberghe P, Nuting L (1933) J Am Chem Soc 55:996
3. Robinson RA, Sinclair DA (1934) J Am Chem Soc 56:1830
4. Robinson RA (1935) J Am Chem Soc 57:1161
5. Robinson RA (1937) J Am Chem Soc 59:84
6. Cudd HH, Felsing WA (1942) J Am Chem Soc 64:550
7. Harned HS, Blander M (1953) J Am Chem Soc 75:2853
8. Mills R, Kennedy JW (1953) J Am Chem Soc 75:5696
9. Mills R (1959) J Phys Chem 63:1873
10. Ti Tien H (1963) J Phys Chem 67:532
11. Horvat J, Bešter-Rogač M, Klofutar C, Rudan-Tasic D (2008) J Solut Chem 37:1329
12. Collins KD (1995) Proc Natl Acad Sci USA 92:5553
13. Dunsmore HS, Jalota SK, Paterson R (1972) J Chem Soc Faraday Trans I 68:1583
14. Khazaeli S, Dye JL, Popov AI (1983) Spectrochim Acta 39A(1):19
15. Afanas'ev VN, Tyunina EY (2003) Russ Chem Bull Int Ed 52(2):336
16. Pan C (1988) J Chem Soc Faraday Trans I 84(5):1341
17. Marcus Y (1997) Ion properties. Marcel Dekker, Inc
18. Chizhik VI, Mikhailov VI, Chong Su P (1987) Theor Exp Chem 22(4):480
19. Ludwig KF Jr, Warburton WK, Fontaine A (1987) J Chem Phys 87(1):620
20. D'Angelo P, Di Nola A, Filipponi A, Pavel N, Roccatano D (1994) J Chem Phys 100(2):985
21. Ascone I, D'Angelo P, Pavel N (1994) J Phys Chem 98:2982
22. D'Angelo P, Di Nola A, Giglio E, Mangoni M, Pavel N (1995) J Phys Chem 99:5471

23. D'Angelo P, Di Nola A, Mangoni M, Pavel N (1996) J Chem Phys 104(5):1779
24. Fulton JL, Pfund DM, Wallen SL, Newville M, Stern EA, Ma Y (1996) J Chem Phys 105(6):2161
25. D'Angelo P, Pavel N (1999) Chem Phys 111(11):5107
26. Ramos S, Barnes AC, Neilson GW, Capitan MJ (2000) Chem Phys 258:171
27. Neilson GW, Mason PE, Ramos S, Sullivan D (2001) Phil Trans R Soc Lond A 359:1575
28. Ohkubo T, Konishi T, Hattori Y, Kanoh H, Fujikawa T, Kaneko K (2002) J Am Chem Soc 124:11860
29. Filipponi A, De Panfilis C, Oliva S, Ricci MA, D'Angelo P, Bowron DT (2003) Phys Rev Lett 91(16), Art. No. 165505
30. D'Angelo P, Persson I (2004) Inorg Chem 43:3543
31. Park C, Fenter PA, Nagy KL, Sturchio NC (2006) Phys Rev Lett 97(1), Art. No. 016101
32. Ansell S, Barnes AC, Mason PE, Neilson GW, Ramos S (2006) Biophys Chem 124:171
33. Harsányi I, Jóvári P, Mészáros G, Pusztai L, Bopp PA (2007) J Mol Liq 131–132:60
34. Harsányi I, Pusztai L (2007) J Phys: Condens Matter 19, Art. No. 335208
35. Ohtaki H, Radnai T (1993) Chem Rev 93(3):1157
36. Adams DJ, Dwyer TM, Hille B (1980) J Gen Physiol 75:493
37. Sheppard JD, Jumarie C, Cooper DG, Laprade R (1991) Biochim Biophys Acta 1064:13
38. Pennefather PS, DeCoursey TE (1994) J Gen Physiol 103:549
39. Teppen BJ, Miller DM (2006) Soil Sci Soc Am J 70:31
40. Van Loon LR, Glaus MA (2008) Environ Sci Technol 42:1600
41. Bezanilla F, Armstrong CM (1972) J Gen Physiol 60:588
42. Doyle DA, Morais-Cabral J, Pfuetzner RA, Kuo A, Gulbis JM, Cohen SL, Chait BT, MacKinnon R (1998) Science 280:69
43. Noskov SY, Bernèche S, Roux B (2004) Nature 431:830
44. Degrève L, Vechi SM, Quintale C Jr (1996) Biochim Biophys Acta 1274:149
45. Laio A, Torre V (1999) Biophys J 76:129
46. Carrillo-Tripp M, Saint-Martin H, Ortega-Blake I (2004) Phys Rev Lett 93(16). Art. No. 168104
47. Carrillo-Tripp M, SanRomán-Zimbrón ML, Hernández-Cobos J, Saint-Martin H, Ortega-Blake I (2006) Biophys Chem 124(3):243
48. Boda D, Nonner W, Henderson D, Eisenberg B, Gillespie D (2008) Biophys J 94:3486
49. Varma S, Sabo D, Rempe SB (2008) J Mol Biol 376:13
50. Miloshevsky GV, Jordan PC (2008) Biophys J 95(7):3239
51. Fowler PW, Tai K, Sansom MSP (2008) Biophys J 95:5062
52. MacKerell AD Jr, Bashford D, Bellott M, Dunbrack RL Jr, Evanseck JD, Field MJ, Fischer S, Gao J, Guo H, Ha S, Joseph-McCarthy D, Kuchnir L, Kuczera K, Lau FTK, Mattos C, Michnick S, Ngo T, Nguyen DT, Prodhom B, Reiher III WE, Roux B, Schlenkrich M, Smith JC, Stote R, Straub J, Watanabe M, Wiórkiewicz-Kuczera J, Yin D, Karplus M (1998) J Phys Chem B 102:3586
53. Daura X, Mark AE, van Gunsteren WF (1998) J Comput Chem 19:535
54. Lee S, Rasaiah JC (1994) J Chem Phys 101(8):6964
55. Lee SH, Rasaiah JC (1996) J Phys Chem 100:1420
56. Koneshan S, Lynden-Bell RM, Rasaiah JC (1998) J Am Chem Soc 120:12041
57. Koneshan S, Rasaiah JC, Lynden-Bell RM, Lee S (1998) J Phys Chem B 102:4193
58. Noworyta JP, Koneshan S, Rasaiah JC (2000) J Am Chem Soc 122:11194
59. Rasaiah JC, Lynden-Bell RM (2001) Phil Trans R Soc Lond A 359:1545
60. Oparin RD, Fedotova MV, Trostin VN (2004) Russ J Gen Chem 74(1):13
61. Harsányi I, Pusztai L, Soetens JC, Bopp PA (2006) J Mol Liq 129:80
62. Pusztai L, Harsányi I, Domínguez H, Pizio O (2008) Chem Phys Lett 457:96
63. Pusztai L, Domínguez H, Pizio O, Sokolowski S (2009) J Mol Liq (in press)
64. Car R, Parrinello M (1985) Phys Rev Lett 55(22):2471
65. Rempe SB, Pratt LR, Hummer G, Kress JD, Martin RL, Redondo A (2000) J Am Chem Soc 122:966
66. Rempe SB, Asthagirib D, Pratt LR (2004) Phys Chem Chem Phys 6:1966
67. Whitfield TW, Varma S, Harder E, Lamoureux G, Rempe SB, Roux B (2007) J Chem Theory Comput 3:2068
68. Leung K, Rempe SB, von Lilienfeld OA (2009) J Chem Phys 130, Art. No. 204507
69. Varma S, Rempe SB (2006) Biophys Chem 124:192
70. Rode BM, Hofer TS (2006) Pure Appl Chem 78(3):525
71. Schwenk CF, Hofer TS, Rode BM (2004) J Phys Chem A 108:1509
72. Warshel A, Levitt M (1976) J Mol Biol 103(2):227
73. Tongraar A, Liedl KR, Rode BM (1998) J Phys Chem A 102:10340
74. Hofer TS, Randolf BR, Rode BM (2005) J Comput Chem 26:949
75. Rode BM, Hofer TS, Randolf BR, Schwenk CF, Xenides D, Vchirawongkwin V (2006) Theor Chem Acc 115:77
76. Azam SS, Hofer TS, Randolf BR, Rode BM (2009) J Phys Chem A 113:1827
77. Pappalardo RR, Martínez JM, Sánchez-Marcos E (1996) J Phys Chem 100(28):11748
78. Martínez JM, Pappalardo RR, Sánchez-Marcos E (1998) J Chem Phys 109(4):1445
79. Martínez JM, Pappalardo RR, Sánchez-Marcos E (1999) J Am Chem Soc 121(3):1669
80. Martínez JM, Hernández-Cobos J, Saint-Martin H, Pappalardo RR, Ortega-Blake I, Sánchez-Marcos E (2000) J Chem Phys 112(5):2339
81. Matsuoka O, Clementi E, Yoshimine M (1976) J Chem Phys 64(4):1351
82. Lie GC, Clementi E, Yoshimine M (1976) J Chem Phys 64(6):2314
83. Saint-Martin H, Hernández-Cobos J, Bernal-Uruchurtu MI, Ortega-Blake I, Berendsen HJC (2000) J Chem Phys 113(24):10899
84. Ren P, Ponder JW (2003) J Phys Chem B 107:5933
85. Fanourgakis GS, Xantheas SS (2008) J Chem Phys 128(7), Art. No. 074506
86. Grossfield A, Ren P, Ponder JW (2003) J Am Chem Soc 125:15671
87. Carrillo-Tripp M, Saint-Martin H, Ortega-Blake I (2003) J Chem Phys 118(15):7062
88. SanRomán-Zimbrón ML, Carrillo-Tripp M, Saint-Martin H, Hernández-Cobos J, Ortega-Blake I (2006) Theor Chim Acc 115:177
89. Lamoureux G, Roux B (2006) J Phys Chem B 110:3308
90. Marcus Y (1994) Biophys Chem 51:111
91. Coe JV (1994) Chem Phys Lett 229:161
92. Tissandier MD, Cowen KA, Feng WY, Gundlach E, Cohen MH, Earhart AD, Coe JV, Tuttle TR Jr (1998) J Phys Chem A 102:7787
93. Schmid R, Miah AM, Sapunov VN (2000) Phys Chem Chem Phys 2:97
94. Kelly CP, Cramer CJ, Truhlar DG (2006) J Phys Chem B 110:16066
95. Hummer G, Pratt LR, García AE (1996) J Phys Chem 100:1206
96. Hummer G, Pratt LR, García AE (1997) J Chem Phys 107(21):9275

97. Figueirido F, Del Buono GS, Levy RM (1995) J Chem Phys 103(14):6133
98. Bogusz S, Cheatham TE III, Brooks BR (1998) J Chem Phys 108(17):7070
99. Kastenholz MA, Hünenberger PH (2006) J Chem Phys 124(12), Art. No. 124
100. Kastenholz MA, Hünenberger PH (2006) J Chem Phys 124(22), Art. No. 224501
101. Warren GL, Patel S (2007) J Chem Phys 127, Art. No. 064509
102. Saint-Martin H, Hernández-Cobos J, Ortega-Blake I (2005) J Chem Phys 122(22), Art. No. 224509
103. Glendening ED, Feller D (1995) J Phys Chem 99:3060
104. Feller D, Glendening ED, Woon DE, Feyereisen MW (1995) J Chem Phys 103(9):3526
105. Dunning TH Jr (1989) J Chem Phys 90(2):1007
106. Hay PJ, Wadt WR (1984) J Chem Phys 82(1):299
107. Feller D (1996) J Comput Chem 17(13):1571
108. Schuchard KL, Didier BT, Elsethagen T, Sun L, Gurumoorthi V, Chase J, Li J, Windus TL (2007) J Chem Inf Model 47(3):1045
109. Džidić I, Kebarle P (1970) J Phys Chem 74(7):1466
110. Park J, Kołaski M, Lee H Myuong, KS Kim (2004) J Chem Phys 121(7):3108
111. Dolg M, Stoll H, Savin A, Preuss H (1989) Theor Chim Acta75:173
112. Nakai H, Klene M, Li X, Knox JE, Hratchian HP, Cross JB, Adamo C, Jaramillo J, Gomperts R, Stratmann RE, Yazyev O, Austin AJ, Cammi R, Pomelli C, Ochterski JW, Ayala PY, Morokuma K, Voth GA, Salvador P, Dannenberg JJ, Zakrzewski VG, Dapprich S, Daniels AD, Strain MC, Farkas O, Malick DK, Rabuck AD, Raghavachari K, Foresman JB, Ortiz JV, Cui Q, Baboul AG, Clifford S, Cioslowski J, Stefanov BB, Liu G, Liashenko A, Piskorz P, Komaromi I, Martin RL, Fox DJ, Keith T, Al-Laham MA, Peng CY, Nanayakkara A, Challacombe M, Gill PMW, Johnson B, Chen W, Wong MW, Gonzalez C, Pople JA (2003) Gaussian 03, Revision B.05. Gaussian, Inc., Pittsburgh
113. Møller C, Plesset MS (1934) Phys Rev 46(7):618
114. Boys SF, Bernardi F (1970) Mol Phys 19(4):553
115. Shank A, Wang Y, Kaledin A, Braams BJ, Bowman JM (2009) J Chem Phys 130, Art. No. 144314
116. Leininger T, Nicklass A, Küchle W, Stoll H, Dolg M, Bergner A (1996) Chem Phys Lett 255:274
117. Weigend F, Ahlrichs R (2005) Phys Chem Chem Phys 7:3297
118. Lotrich VF, Salewicz K (1997) J Chem Phys 106(23):9668
119. Tóth G (1996) J Chem Phys 105(13):5518
120. Dang LX (1992) J Chem Phys 96(9):6970
121. Ayala R, Martínez JM, Pappalardo RR, Saint-Martin H, Ortega-Blake I, Sánchez-Marcos E (2002) J Chem Phys 117(23):10512
122. Spångberg D, Hermansson K (2003) J Chem Phys 119(14):7263
123. Metropolis N, Rosenbluth AW, Rosenbluth MN, Teller AH, Teller E (1953) J Chem Phys 21:1087
124. Hastings WK (1970) Biometrika 57:92
125. Ewald PP (1921) Ann Phys 64:253
126. Soper AK (2001) Mol Phys 99(17):1503
127. Evans R (1998) Mol Sim 4:409
128. Stern HA, Berne BJ (2001) J Chem Phys 115(16):7622
129. Guillot B (2002) J Mol Liq 101(1–3):219
130. Paesani F, Voth GA (2009) J Phys Chem B 113:5702
131. Sesé LM (1994) Mol Phys 81(6):1297
132. Guillot B, Guissani Y (1998) J Chem Phys 108(24):10162
133. Guillot B, Guissani Y (2001) J Chem Phys 114(15):6720
134. Tunell I, Lim C (2006) Inorg Chem 45:4811
135. Newsome JR, Neilson GW, Enderby JE (1980) J Phys C 13:L923
136. Asthagiri D, Pratt LR, Ashbaugh HS (2003) J Chem Phys 119(5):2702
137. Grossfield A (2005) J Chem Phys 122, Art. No. 024506
138. Zhan C, Dixon DA (2001) J Phys Chem A 105(51):11534
139. Fawcett WR (1999) J Phys Chem B 103:11181
140. Rais JR, Okada T (2006) Anal Sci 22:533
141. Flyvbjerg H, Petersen HG (1989) J Chem Phys 91(1):461
142. Straatsma TP, Berendsen HJC (1988) J Chem Phys 89:5876
143. Berendsen HJC, Grigera JR, Straatsma TP (1987) J Phys Chem 91:6269